Modeling the Neuroprotective Role of Enhanced Astrocyte Mitochondrial Metabolism during Stroke

Casey O. Diekman,[†*] Christopher P. Fall,[‡§] James D. Lechleiter,[¶] and David Terman[‖]
[†]Mathematical Biosciences Institute, The Ohio State University, Columbus, Ohio; [‡]Department of BioEngineering, University of Illinois at Chicago, Chicago, Illinois; [§]Department of Computer Science, Georgetown University, Washington, District of Columbia; [¶]Department of Cellular and Structural Biology, University of Texas Health Science Center at San Antonio, San Antonio, Texas; and [‖]Department of Mathematics, The Ohio State University, Columbus, Ohio

ABSTRACT A mathematical model that integrates the dynamics of cell membrane potential, ion homeostasis, cell volume, mitochondrial ATP production, mitochondrial and endoplasmic reticulum Ca^{2+} handling, IP_3 production, and GTP-binding protein-coupled receptor signaling was developed. Simulations with this model support recent experimental data showing a protective effect of stimulating an astrocytic GTP-binding protein-coupled receptor ($P2Y_1Rs$) following cerebral ischemic stroke. The model was analyzed to better understand the mathematical behavior of the equations and to provide insights into the underlying biological data. This approach yielded explicit formulas determining how changes in IP_3-mediated Ca^{2+} release, under varying conditions of oxygen and the energy substrate pyruvate, affected mitochondrial ATP production, and was utilized to predict rate-limiting variables in $P2Y_1R$-enhanced astrocyte protection after cerebral ischemic stroke.

INTRODUCTION

Acute cerebral ischemia causes cytotoxic edema in neurons, glia, and endothelial cells, with swelling being most prominent in astrocytes (1–3). Within minutes of hypoxia, failure of ATP-dependent ion transport leads to rapid accumulation of sodium and chloride ions inside the cell. Water flows into the cell to maintain osmotic equilibrium, causing the cell to swell. Zheng et al. (4) showed that, in mouse cortical astrocytes, the magnitude of ischemic lesions and cytotoxic edema were significantly reduced by treatment with the purinergic ligand 2-methylthioladenosine 5′ diphosphate (2MeSADP), an agonist with high specificity for the purinergic receptor type-1 isoform ($P2Y_1R$). We previously reported that stimulation of $P2Y_1Rs$ increases calcium-sensitive mitochondrial metabolism in astrocytes (5). These data suggest that astrocyte mitochondria are a key energy source in postischemic tissue, and can be stimulated by IP_3-mediated intracellular Ca^{2+} release to significantly improve neurological outcomes subsequent to brain injuries (Fig. 1).

We tested this hypothesis by constructing a mathematical model of an astrocyte that integrates cellular membrane potential and volume with models of mitochondrial ATP production and endoplasmic reticulum (ER) calcium handling. In our model, we can induce cellular swelling and depolarization by decreasing parameters corresponding to either the overall glucose level or the supply of oxygen. Simulations of the model demonstrate that ischemia-induced cell swelling and depolarization can be reversed by enhancing IP_3-mediated Ca^{2+} release, which increases mitochondrial ATP production.

We also mathematically analyze the model to better understand mechanisms underlying the experimental results and model behavior. In particular, what critical fluxes play a decisive role in the generation of ischemic-like conditions and how does the model's ability to reverse cell swelling and depolarization depend on parameters? We systematically simplify the model, and derive a reduced model that not only reproduces the full model's behavior but is also considerably easier to analyze mathematically. Using the reduced model, we derive explicit formulas that predict how changes in IP_3-mediated Ca^{2+} release, pyruvate level, and external oxygen level affect mitochondrial ATP production.

METHODS

A schematic of the model is shown in Fig. 1. The model combines the Magnus-Keizer model for mitochondrial Ca^{2+} handling and ATP production (6,7) and the Li-Rinzel model for Ca^{2+}-handling in the ER (8) together with models for the $P2Y_1R$ (which stimulates IP_3 production), Na^+/K^+ pump, cell volume and cell membrane potential. To study how ATP production depends on the overall glucose and oxygen levels, and the role of other processes in neuroprotection, we have made several modifications to the Magnus-Keizer model:

1. Whereas ATP production is a dynamical variable in the Magnus-Keizer model, the oxygen level is a fixed parameter. For this reason, it is necessary to modify the model so that oxygen input is a parameter and the oxygen level in the mitochondria is a dynamical variable.
2. Recent experiments have demonstrated that mitochondrial K_{ATP} channels play an important role in controlling the mitochondrial membrane potential and, therefore, ATP production (9,10). We have added a K_{ATP} channel to the Magnus-Keizer model to explore its possible role in neuroprotection.
3. Finally, neurons are considerably less tolerant to changes in glucose and oxygen levels than are astrocytes (11). This may be because of the so-called permeability transition pore (PTP), which plays a much more prominent role in neurons than in astrocytes. The PTP is important in mitochondrial Ca^{2+} handling and metabolism/energetics in neurons

Submitted July 6, 2012, and accepted for publication February 8, 2013.

*Correspondence: cdiekman@gmail.com

Editor: Michael Stern.

0006-3495/13/04/1752/12 $2.00

http://dx.doi.org/10.1016/j.bpj.2013.02.025

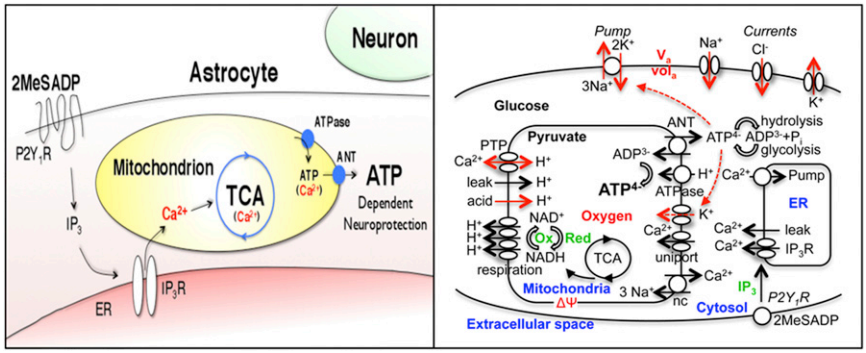

FIGURE 1 Diagram of neuroprotective role of enhanced astrocyte mitochondrial metabolism. (*Left*) $P2Y_1R$ ligands stimulate IP_3-mediated calcium release from the ER of astrocytes, which increases mitochondrial calcium levels leading to the increased production of ATP and neuroprotection. (*Right*) Schematic of computational model of ER-mitochondrial calcium handling, ATP production, and cell swelling.

(but not astrocytes), because it releases Ca^{2+} and dissipates $\Delta\Psi$ when open. To study neuroprotection in neurons, we have modified the Magnus-Keizer model by adding a recently developed model for the PTP (12). Details of our modifications to the Magnus-Keizer model are described below.

The modified Magnus-Keizer model

For mitochondrial Ca^{2+} handling and ATP production, we use the model developed by Magnus and Keizer (7), with several modifications. Here we describe the modified model for mitochondria within astrocytes. The neuron model, in which we add the PTP, is given later.

The modified model can be written as

$$\frac{d[\mathrm{NADH}]_m}{dt} = \frac{m\left(J_{pdh} - J_o\right)}{\gamma_\mu \tau_{min} vol_m}, \tag{1}$$

$$\frac{d[\mathrm{ADP}]_m}{dt} = \frac{m\left(J_{ant} - J_{ptca} - J_{pf1}\right)}{\gamma_\mu \tau_{min} vol_m}, \tag{2}$$

$$\frac{d\Delta\Psi}{dt} = \frac{m\left(J_{hres} - J_{hf1} - J_{ant} - J_{hl} - J_{Katp} - 2J_{uni} + J_{nc}\right)}{\tau_{min} C_m}, \tag{3}$$

$$\frac{d[\mathrm{Ca}]_m}{dt} = \frac{f_m m\left(J_{uni} - J_{nc}\right)}{\tau_{min} vol_m}, \tag{4}$$

$$\frac{d[\mathrm{ADP}]_c}{dt} = -\frac{mJ_{ant} + c\left(J_{hyd} - J_{pgly}\right)}{\gamma_\mu \tau_{min} vol_c}, \tag{5}$$

$$\frac{d[\mathrm{H}]_m}{dt} = \frac{f_{hm} m\left(J_{hf1} + J_{hl} - J_{hres} + J_{ah}\right)}{\tau_{min} vol_m}, \tag{6}$$

where the subscript m corresponds to a mitochondrial component and the subscript c corresponds to a cytosolic component. The variable $\Delta\Psi$ represents the electrochemical gradient of the mitochondrion relative to the cytosol. An interpretation of the various fluxes in this model can be found in Magnus and Keizer (7) or Oster et al. (12). The constants m, c, f_m, C_m, vol_m, and vol_c, represent the amount of mitochondrial proteins, the amount of cytosolic proteins, mitochondrial Ca^{2+} buffering, mitochondrial inner membrane capacitance, mitochondrial volume, and cytosolic volume, respectively. Note that the amount of ATP in the mitochondrion and cytosol are determined by the conservation equations

$$[\mathrm{ATP}]_m = A_{mtot} - [\mathrm{ADP}]_m \text{ and } [\mathrm{ATP}]_c = A_{ctot} - [\mathrm{ADP}]_c, \tag{7}$$

respectively, where A_{mtot} and A_{ctot} are constants.

Here, we will only describe our modifications to fluxes in the Magnus-Keizer model. A detailed description of the various fluxes and parameter values is given in the Supporting Material.

The first modification to the Magnus-Keizer model was suggested by Bertram et al. (13). In the Magnus-Keizer model, it is assumed that the rate at which NADH is produced by the citric-acid cycle is proportional to the reaction rate of the pyruvate dehydrogenase complex (PDH). In that model, this rate is represented by J_{red}, which is a function of mitochondrial calcium. As in Bertram et al. (13), we replace J_{red} with J_{pdh}, which has explicit dependence on both $[\mathrm{Ca}]_m$ and the ratio of product NADH to substrate NAD^+. The input to the PDH is pyruvate, which is converted from glucose via glycolysis in the cytosol. Thus, we make J_{pdh} dependent on the cytosolic glucose concentration, GLC. The expression for J_{pdh} is

$$J_{pdh} = \left(\frac{p_a}{p_b + [\mathrm{NADH}]_m/[\mathrm{NAD}]_m}\right)\left(\frac{[\mathrm{Ca}]_m}{p_c + [\mathrm{Ca}]_m}\right)J_{pyr},$$

where

$$J_{pyr} = k_{pyr}\sqrt{GLC} \text{ and } [\mathrm{NAD}]_m = N_{tot} - [\mathrm{NADH}]_m, \tag{8}$$

and N_{tot} is a constant.

For the second modification, we introduce a dynamical variable, O, corresponding to the level of oxygen inside the mitochondrion. In the Magnus-Keizer model, oxygen is a static parameter that appears in two fluxes: respiration and oxygen consumption. If we denote the original Magnus-Keizer formulation of these fluxes as $\hat{J}_{hres}$ and $\hat{J}_o$, then we take the modified fluxes to be

$$J_{hres} = \left(\frac{O}{k_o + O}\right)\hat{J}_{hres} \text{ and } J_o = \left(\frac{O}{k_o + O}\right)\hat{J}_o,$$

where k_o is a constant. We then assume that O satisfies the differential equation

$$\frac{dO}{dt} = d(O_{out} - O) - \alpha J_O, \tag{9}$$

where O_{out} is the oxygen level outside the mitochondrion, d is a diffusion constant, and α is a rate parameter.

Mitochondrial pH is also static in the Magnus-Keizer model. As in Oster et al. (12), we have added a differential equation to track changes in $[\mathrm{H}]_m$, the mitochondrial proton concentration. This will be especially

important when we consider the PTP, the opening of which depends on the mitochondrial pH level. The Magnus-Keizer model contains three H^+ fluxes: respiration, the FoF1 ATPase, and a $\Delta\Psi$-dependent leak term. To these we have added a term J_{ah} that corresponds to an electroneutral inorganic phosphate flux; this flux serves as a weak acid and provides a mechanism for mitochondrial pH buffering.

We model the ATP-sensitive K^+ current, J_{Katp}, as in Bertram et al. (14) and Magnus and Keizer (15),

$$J_{Katp} = g_{Katp} o_\infty\left([\mathrm{ADP}]_m, [\mathrm{ATP}]_m\right)(\Delta\Psi - \Psi_K). \quad (10)$$

Here, g_{Katp} is the maximal conductance, Ψ_K is the equilibrium potential of K^+ and

$$o_\infty\left([\mathrm{ADP}]_m, [\mathrm{ATP}]_m\right) = \frac{0.08\left(1+\frac{2MgADP^-}{17}\right)+0.89\left(\frac{MgADP^-}{17}\right)^2}{\left(1+\frac{MgADP^-}{17}\right)^2\left(1+\frac{ADP^{3-}}{26}+ATP^{4-}\right)},$$

where

$$MgADP^- = 0.165[\mathrm{ADP}]_m,\ ADP^{3-} = 0.135[\mathrm{ADP}]_m,\ \text{and}\ ATP^{4-} = 0.05[\mathrm{ATP}]_m.$$

Finally, we modified the Ca^{2+} uniporter J_{uni}. With its original formulation, J_{uni} sometimes becomes slightly negative during some of the simulations. Because it is unclear whether this is possible over the range of conditions considered here, we simply assume that if $\widehat{J}_{uni}$ is the original Magnus-Keizer formulation of the Ca^{2+} uniporter, then $J_{uni} = \widehat{J}_{uni}$ if $\widehat{J}_{uni}>0$ and $J_{uni} = 0$ otherwise. We note that all of the results presented in this article hold without this modification.

Cytosolic Ca^{2+}

We will distinguish between two forms of cytosolic Ca^{2+}. The first is the overall amount of Ca^{2+} in the cell not bound to buffers; we denote this as $[\mathrm{Ca}]_c$ and assume that it is constant (though the general case would include plasma membrane Ca^{2+} fluxes). The second is the amount of free Ca^{2+} that lies between the IP_3 receptor pore and the mitochondria's Ca^{2+} uniporter; we denote the concentration of Ca^{2+} in this space as $[\mathrm{Ca}]_{ps}$, for pore-space Ca^{2+}. Then $[\mathrm{Ca}]_{ps}$ satisfies the differential equation,

$$\frac{d[\mathrm{Ca}]_{ps}}{dt} = \frac{f_{ps}(m(J_{nc}-J_{uni}) - e(J_{serca}-J_{erout}))}{vol_{ps}}, \quad (11)$$

where f_{ps} is Ca^{2+} buffering in the pore space. Note that the total amount of Ca^{2+} in the ER, mitochondria, and the pore space between them is conserved; that is,

$$[\mathrm{Ca}]_{ps} = \frac{f_{ps}}{vol_{ps}}\left([\mathrm{Ca}]_{tot} - \frac{vol_m}{f_m}[\mathrm{Ca}]_m - \frac{vol_{er}}{f_e}[\mathrm{Ca}]_{er}\right).$$

We note that there should be diffusion between the cytosolic and pore-space Ca^{2+}. However, we assume that this is dominated by the other Ca^{2+} fluxes and can, therefore, be ignored.

ER dynamics

Our model for Ca^{2+}-handling in the ER is the same as that proposed by Li and Rinzel (8), except we add a dynamic variable to account for $P2Y_1R$ binding and IP_3 degradation. The Li-Rinzel model can be written as

$$\frac{d[\mathrm{Ca}]_{er}}{dt} = \frac{f_e e(J_{serca}-J_{erout})}{\tau_{min} vol_{\mathrm{er}}}, \quad (12)$$

$$\frac{dh}{dt} = \frac{d_{inh} - \left([\mathrm{Ca}]_{ps}+d_{inh}\right)h}{\tau}, \quad (13)$$

where e and f_e represent ER protein amount and Ca^{2+} buffering,

$$J_{erout} = \left[J_{max}^{ip3}\left(\frac{[\mathrm{IP_3}]}{[\mathrm{IP_3}]+d_{ip3}}\right)^3\left(\frac{[\mathrm{Ca}]_{ps}}{[\mathrm{Ca}]_{ps}+d_{act}}\right)^3 h^3 + J_{leak}\right] \times\left([\mathrm{Ca}]_{er}-[\mathrm{Ca}]_{ps}\right)$$

and

$$J_{serca} = \frac{v_{serca}[\mathrm{Ca}]_{ps}^2}{k_{serca}^2+[\mathrm{Ca}]_{ps}^2}$$

represent the release of Ca^{2+} from the ER through IP_3 channels and intake of Ca^{2+} into the ER through the SERCA pump, respectively, and h is a variable for slow inactivation of the channel.

In the Li-Rinzel model, $[\mathrm{IP_3}]$ is a constant, and is set between 0.3 and 0.6 μM in the simulations in their article (8). The dynamics of $[\mathrm{IP_3}]$, including Ca^{2+}-dependent IP_3 production pathways, have been modeled by Fall et al. (16). Here we follow Di Garbo et al. (17), and assume that $[\mathrm{IP_3}] = (0.45 + [\mathrm{IP_3}]_a)$ μM, where $[\mathrm{IP_3}]_a$ is a dynamic variable that satisfies a differential equation of the form

$$\frac{d[\mathrm{IP_3}]_a}{dt} = k_{P2Y}x_F - k_{deg}[\mathrm{IP_3}]_a, \quad (14)$$

and where

$$x_F = \frac{MeS}{K_D+MeS}$$

is the fraction of metabotropic ATP receptors bound. The term $k_{P2Y}x_F$ represents the rate of IP_3 production promoted through the G-protein and PLCβ activation pathway in a stimulated cell.

Note that stimulation of the $P2Y_1R$ (by increasing MeS, the parameter representing application of 2MeSADP) leads to an increase in IP_3, which increases J_{erout} and, therefore, $[\mathrm{Ca}]_{ps}$. As diagrammed in Fig. 1, this, in turn, leads to an increase in $[\mathrm{Ca}]_m$. As we demonstrate later, this has the

potential to increase ATP production and reverse the effects of ischemia on cell volume and membrane potential.

Model of cell volume and membrane potential

We assume that changes in the cell volume are due to the flow of water with ions at just the rate sufficient to maintain isotonicity between the cell's interior and exterior. Here, we will consider just three ions: Na^+, K^+, and Cl^-, whose concentrations change due to voltage-gated channels and Na^+/K^+ pumps. Other ions such as Ca^{2+} and glutamate certainly play a critical role in ischemia, as do other pumps and transporters (18). However, a detailed model and analysis of interactions between these complex processes is beyond the scope of this article. Although mitochondrial volume is osmotically active (19), here we assume that the volumes of the organelles and the pore space are constant. Our minimal model is still capable of demonstrating the role of mitochondrial Ca^{2+} sequestration in maintaining proper ATP production and how reductions in ATP production lead to cell swelling and collapse of the cell membrane potential.

Let Na_i, K_i, and Cl_i be the amounts of intracellular Na^+, K^+, and Cl^- ions, respectively. Then the change in cell volume is given by

$$\frac{d(vol_a)}{dt} = \frac{1}{[\mathrm{E}]_0}\left(\frac{dNa_i}{dt} + \frac{dK_i}{dt} + \frac{dCl_i}{dt}\right), \tag{15}$$

where $[\mathrm{E}]_o$ is the total extracellular solute concentration (20). Hence,

$$vol_a(t) = \frac{1}{[\mathrm{E}]_o}(Na_i(t) + K_i(t) + Cl_i(t)) + \kappa_1,$$

where κ_1 is a constant that depends on initial conditions. Moreover, to satisfy the internal electroneutrality condition, we have that

$$\frac{dCl_i}{dt} = \frac{dNa_i}{dt} + \frac{dK_i}{dt} \tag{16}$$

or

$$Cl_i(t) = Na_i(t) + K_i(t) - \kappa_2,$$

where κ_2 is another constant that depends on initial conditions. It therefore remains to describe equations for $Na_i(t)$ and $K_i(t)$. We assume that the ionic currents satisfy the Goldman-Hodgkin-Katz current equation and that there is a Na^+/K^+ pump. Then these variables satisfy the differential equations

$$\frac{dNa_i}{dt} = A\left(\frac{P_{Na}\phi\left([\mathrm{Na}]_o - [\mathrm{Na}]_i \exp(\phi)\right)}{\exp(\phi) - 1} - I_{pump}\right), \tag{17}$$

$$\frac{dK_i}{dt} = A\left(\frac{P_K\phi\left([\mathrm{K}]_o - [\mathrm{K}]_i \exp(\phi)\right)}{\exp(\phi) - 1} + I_{pump}\right), \tag{18}$$

where $\phi = FV_a/RT$. V_a is the membrane potential of the astrocyte, P_{Na} and P_K are permeabilities, A is the membrane surface area, S_i is the amount of internal S ions, and $[\mathrm{S}]_i$, $[\mathrm{S}]_o$ are the internal and external concentrations, respectively (20). We assume that activity of the Na^+/K^+ pump depends on $[\mathrm{ATP}]_c$:

$$I_{pump} = \frac{K[\mathrm{Na}]_i}{\rho}\left(1 + \tanh\left(\frac{[\mathrm{ATP}]_c - 1.93}{0.1}\right)\right). \tag{19}$$

Finally, we assume that the membrane potential satisfies the Goldman-Hodgkin-Katz voltage equation (21):

$$V_a = \frac{RT}{F}\, ln\left(\frac{P_{Na}[\mathrm{Na}]_o + P_K[\mathrm{K}]_o + P_{Cl}[\mathrm{Cl}]_i}{P_{Na}[\mathrm{Na}]_i + P_K[\mathrm{K}]_i + P_{Cl}[\mathrm{Cl}]_o}\right). \tag{20}$$

Model simulations were performed using MATLAB (22) and XPPAUT (23). Bifurcation diagrams were computed using XPPAUT.

RESULTS

Simulations of ischemia and recovery in astrocytes

A standard in vitro model of ischemia is oxygen and glucose deprivation (24). We simulated ischemia in our mathematical model by reducing the amount of cytosolic glucose and oxygen (parameters *GLC* and O_{out}, respectively).

Fig. 2 shows the effect of reduced glucose on mitochondrial ATP concentration, cell membrane potential, and cell volume. In the control state (the first 20 min of simulation), the membrane potential and volume of the astrocyte were steady near −80 mV and 7500 μm^3, respectively. At $t = 20$ min, *GLC* was lowered by 25%. This led to a decrease in ATP production and thus decreased activity of the ATP-dependent Na^+/K^+ pump. The altered ion transport caused the astrocyte to depolarize to ~−20 mV, and the astrocyte volume to increase by 80%. Stimulation of the $P2Y_1R$ can reverse these effects, as shown in Fig. 3. We again started with the model in the control state and induced ischemia at $t = 20$. At $t = 40$, we increased the value of the parameter *MeS* from 0 to 0.04 to simulate application of 2MeSADP.

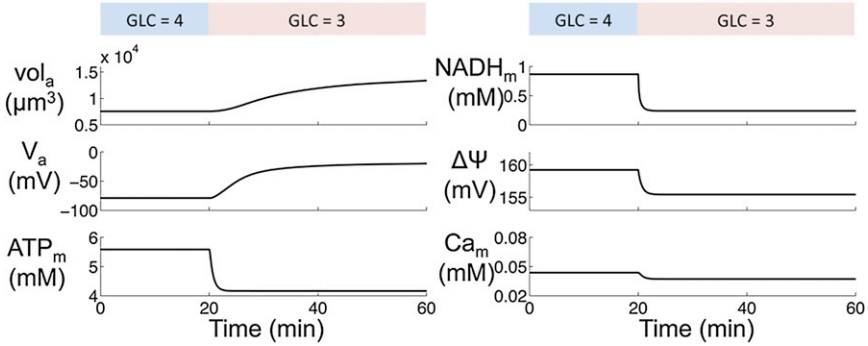

FIGURE 2 Simulation of ischemia. At $t = 20$ min, cytosolic glucose concentration is suddenly reduced by 25%. ATP production falls, leading to cell depolarization and swelling.

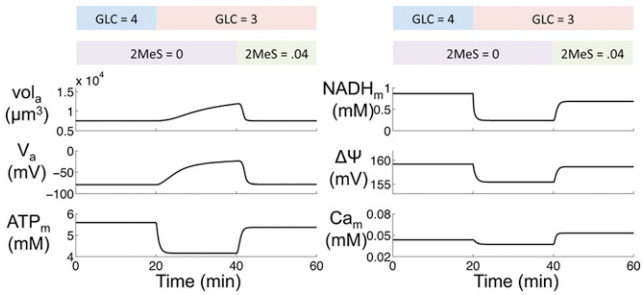

FIGURE 3 Simulation of recovery from glucose deprivation. At t = 40 min, $P2Y_1R$ receptor is stimulated, leading to an increase in mitochondrial calcium concentration, ATP production, and reversal of cell depolarization and swelling.

This led to an increase in mitochondrial Ca^{2+}, which restored ATP production to near the control-state level. The membrane potential hyperpolarized to near −80 mV, and the volume of the astrocyte shrank back to its original value.

Similar effects are seen when we simulate a reduction in oxygen supply. Fig. 4 shows a 50% reduction in O_{out}, which leads to a drop in ATP production, membrane depolarization, and cell swelling, and the partial reversal of these effects by stimulation of the $P2Y_1R$ ($MeS = 0.04$). Full recovery can be achieved by stronger stimulation of $P2Y_1R$ ($MeS = 0.1$), as shown in Fig. 5. Here, stroke was simulated by the simultaneous reduction of both GLC and O_{out}. In this case, application of 2MeSADP led to oscillations during the recovery phase. There is experimental evidence for calcium-dependent oscillations in mitochondrial transmembrane potential ($\Delta\Psi$) in cultures of SH-SY5Y human neuroblastoma cells (25). Furthermore, oscillations in IP_3 have been observed in astrocytes in response to stimulation of $P2Y_1Rs$ by extracellular ATP (26). In our model, oscillations are observed for certain combinations of MeS, GLC, and O_{out}. For example, with $MeS = 0.04$ and $O_{out} = 1$, the model exhibits oscillations in ATP_m production if $GLC \leq 2$ (see Fig. S2 in the Supporting Material). Thus, the relationship between GLC and the amount of depolarization and swelling (averaged over the last 5 min of simulation) is not monotonic for this value of MeS. This nonmonotonicity is a prediction of the model that could be tested experimentally.

To explore further the ability of $P2Y_1R$ stimulation to counter astrocyte depolarization and swelling during stroke, we simulated different levels of glucose or oxygen supply and 2MeSADP application. Fig. 6 demonstrates that ischemic-like conditions arise if MeS and either GLC or O_{out} levels are sufficiently small. Moreover, except for very low values of GLC and O_{out}, membrane potential and cell volume return to their control state with elevated values of MeS.

For the simulations shown in Figs. 2–6, we did not include the mitochondrial K_{ATP} channel. As Fig. 7 illustrates, addition of this channel makes the astrocyte less vulnerable to a decrease in the glucose level (a similar result holds for a decrease in the oxygen level), and enhances the neuroprotective role of 2MeSADP application. In Fig. 7, A and B, we initiate ischemia at $t = 500$ s by decreasing GLC by 25%. Note that the subsequent drop in $[ATP]_c$ is a decreasing function of g_{Katp}, the maximal conductance of the K_{ATP} current. At $t = 1000$, we increase MeS. For the simulation shown in Fig. 7 A, MeS is chosen to be small so that there is only partial recovery from ischemia. As expected, the recovery level increases with g_{Katp}. A larger value for MeS is used in Fig. 7 B and the system fully recovers for all values of g_{Katp}.

The mitochondrial permeability transition pore

Neurons are considerably more vulnerable to changes in ischemic conditions than astrocytes (11). One possible explanation for this is that the permeability transition pore, which both releases Ca^{2+} and is directly or indirectly responsive to Ca^{2+}, plays a much more prominent role in neurons than in astrocytes. The PTP has been the nexus of a large experimental effort principally because it appears that permanent activation of the transition and subsequent depolarization of mitochondria constitutes an obligate initiating step to most nonreceptor-mediated programmed cell

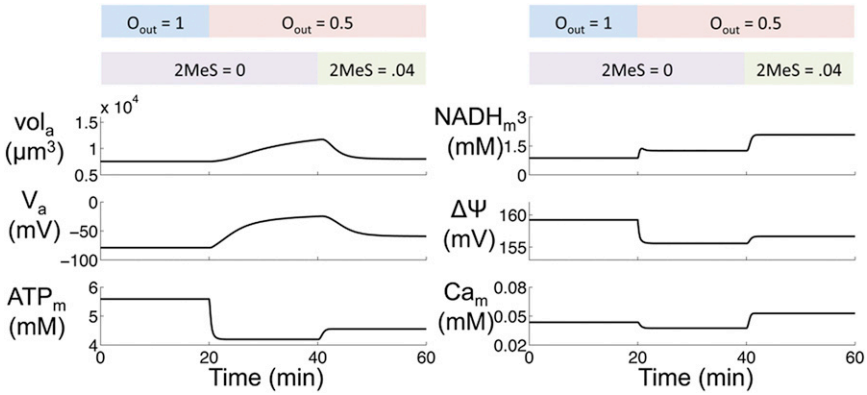

FIGURE 4 Simulation of partial recovery from oxygen deprivation. At $t = 40$ min, $P2Y_1R$ receptor is stimulated, leading to an increase in mitochondrial calcium concentration, ATP production, and reversal of cell depolarization and swelling.

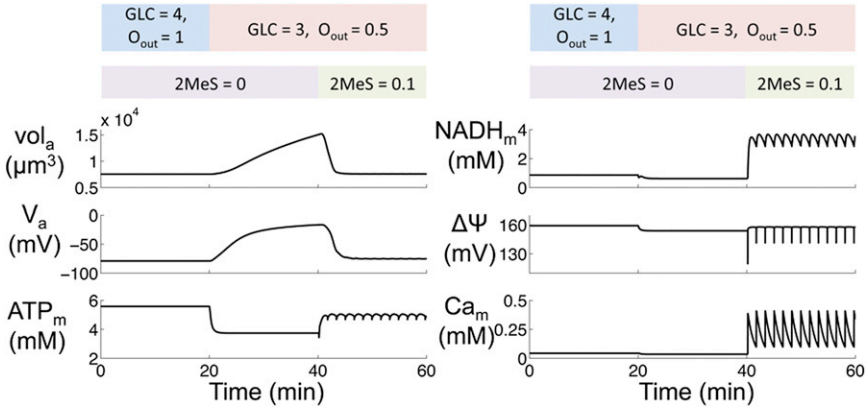

FIGURE 5 Oscillations during recovery from simulated ischemia. At $t = 20$ min, glucose and oxygen supply are reduced simultaneously. At $t = 40$ min, $P2Y_1R$ receptor is stimulated, leading to oscillatory behavior and the reversal of cell depolarization and swelling. The dynamics of the model fluxes during this simulation are shown in Fig. S1 in the Supporting Material.

death. The PTP may have two open states sensitive to different stressors: there is a transient, low conductance state and a high conductance state with irreversible opening. Players known to affect the open probability of the PTP are many of the same factors that are implicated in cell death in both health and disease: Ca^{2+}, pH, reactive oxygen species, altered membrane lipids, electron transport chain anomalies, and altered gene expression.

To explore differences in the vulnerability of neurons and astrocytes to ischemic conditions, we incorporate a recently developed model for the PTP (12). Here, we only consider the PTP low-conductance state. This is modeled as follows: Let PTP_l denote the number of PTP channels that are in the low conductance state. We assume that the dynamics of the low-conductance state depend upon pH and are governed by

$$\frac{dPTP_l}{dt} = \frac{PTP_l^{\infty}\left([\mathrm{H}]_m\right) - PTP_l}{\tau_l\left([\mathrm{H}]_m\right)}. \tag{21}$$

Both the opening rate, PTP_l^{∞}, and the time constant, τ_1, depend upon the mitochondrial proton concentration $[\mathrm{H}]_m$—that is, mitochondrial pH. In particular, we take

$$PTP_l^{\infty} = 0.5\left(1 + \tanh\left(\frac{p_1 - [\mathrm{H}]_m}{p_2}\right)\right)$$

and

$$\tau_l\left([\mathrm{H}]_m\right) = \frac{A_\tau}{\cosh\left(\frac{[\mathrm{H}]_m - p_3}{p_4}\right)} + p_6.$$

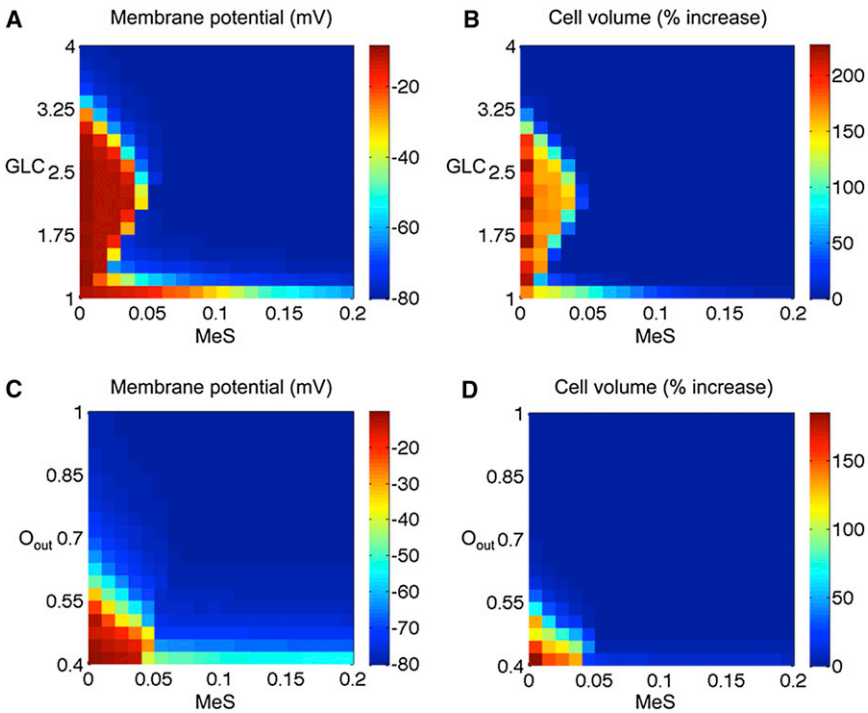

FIGURE 6 (*Top*) Cell membrane potential (*A*) and volume (*B*) for different values of glucose supply and *MeS*. (*Bottom*) Cell membrane potential (*C*) and volume (*D*) for different values of oxygen supply and *MeS*. In all cases, the cell was simulated in a control state ($GLC = 4$, $O_{out} = 1$, $MeS = 0$) for 20 min. An ischemic state was then induced by either reducing *GLC* or O_{out} or the value shown along the vertical axes for 20 min, while keeping $MeS = 0$. Finally, *MeS* was increased to the value shown along the horizontal axes for 20 min. The reported membrane potential and volume correspond to the average V_a and vol_a values over the last 5 min of simulation.

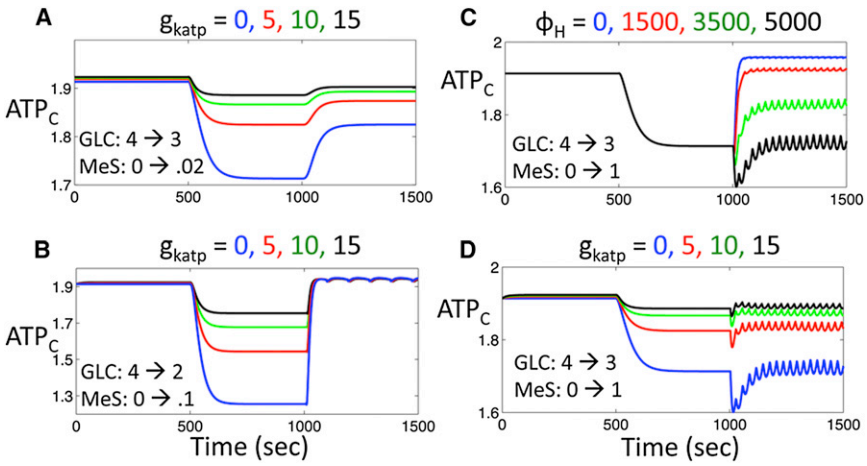

FIGURE 7 (*A*) Increasing the maximal conductance of the K_{ATP} current leads to a smaller drop in cytosolic ATP production during stroke-like conditions and enhances the neuroprotective role of 2MeSADP application. Here, there is no PTP. (*B*) If *MeS* is sufficiently large, then the system fully recovers for all values of g_{Katp}. (*C*) Addition of the PTP makes the astrocyte more vulnerable to decreases in glucose levels and weakens the neuroprotective role of 2MeSADP application. Here, g_{Katp}. (*D*) Similar to panel *A*, except the PTP is now included. Here, $\phi_H = 5000$.

Note that p_1 is the parameter that primarily determines whether the pore is open or closed. That is, the pore opens when $[H]_m$ falls to $<p_1$ and closes when $[H]_m$ is $>p_1$. For the simulations shown below, $p_1 = 0.024$. The other constants p_i and A_τ are given in the Supporting Material.

We assume that the PTP is permeable to protons and Ca^{2+} when open. The proton flux is taken to be of the Goldman-Hodgkin-Katz form gated by the state of the pore:

$$J^H_{PTP} = \phi_H PTP_i \frac{F\Delta\Psi}{RT}\left([H]_m - [H]_c \frac{\exp\left(\frac{-F\Delta\Psi}{RT}\right)}{1-\exp\left(\frac{-F\Delta\Psi}{RT}\right)}\right).$$

Here, $[H]_c$ is the cytosolic proton concentration, which we assume is constant, and ϕ_H is the permeability of the pore in its low-conductance state to protons. Very little is known in regard to the Ca^{2+} flux through the PTP. Here, we assume that this flux uses the same expression as flux through the uniporter from the Magnus-Keizer model and is gated by the state of the pore. That is,

$$J^{Ca}_{PTP} = \phi_{Ca} PTP_i J_{uni}\left([Ca]_c, [Ca]_m\right).$$

To complete the model, we add the fluxes $(2J^{Ca}_{PTP} - J^H_{PTP})$, $-J^{Ca}_{PTP}$ and J^H_{PTP} to the right-hand sides of Eqs. 3, 4, and 6 for $\Delta\Psi$, $[Ca]_m$, and $[H]_m$, respectively.

As Fig. 7 *C* illustrates, addition of the PTP makes the astrocyte more vulnerable to decreases in glucose and oxygen levels, and weakens the neuroprotective role of 2MeSADP application. As before, strengthening the K_{ATP} current makes the cell less vulnerable to decreases in glucose, even in the presence of the PTP. This is illustrated in Fig. 7 *D*.

Fig. 8 shows the time courses of dependent variables for the model without the PTP ($\phi_H = \phi_{Ca} = 0$, *blue curves*) and with the PTP ($\phi_H = 5000$, $\phi_{Ca} = 0$, *red curves*). The system is at its control state until $t = 500$ s, at which time we simulate stroke-like conditions by lowering *GLC* from 4 to 2. At $t = 1000$, we increase *MeS* from 0 to 1. Note that the PTP opens shortly after MeS is increased (see J_{ptp}). This leads to lower values of $[NADH]_m$, $\Delta\Psi_m$, and $[ATP]_m$. Recall that the PTP becomes activated whenever $[H]_m$ falls to $<p_1 = 0.024$. As the figure illustrates, this occurs periodically, leading to oscillations in the PTP flux, J_{ptp}. Fig. 8 also shows projections of the solution onto three-dimensional phase spaces. Note that as soon as *MeS* is increased, there is a sharp drop in both $\Delta\Psi$ and $[H]_m$, due to the initial increase in mitochondrial Ca^{2+}, followed by recovery of both of these variables. It is this sharp drop in $[H]_m$ that leads to the initial opening of the PTP.

Simplification of the model

We wanted to analyze the full model mathematically to better understand mechanisms and conditions for when changes in glucose, oxygen, and $P2Y_1R$ stimulation levels lead to enhanced or diminished ATP production. However, the expressions for the fluxes in the modified Magnus-Keizer model are extremely complicated. For this reason, we have systematically simplified fluxes for the mitochondrial variables to a form that is amenable to mathematical analysis. In the simplified model, we assume that the pH is constant, as was done in the original Magnus-Keizer model. Hence, the simplified Magnus-Keizer model for the mitochondrial variables reduces to equations for $[Ca]_m$, $\Delta\Psi$, $[NADH]_m$, and $[ADP]_m$. A detailed description of the simplified expressions is given in the Supporting Material.

In numerical simulations, the simplified Magnus-Keizer model produces very similar dynamics to that of our full model (see Fig. S3). Because we have eliminated the cytosolic variables, in the simplified Magnus-Keizer model we adjust pyruvate concentration (Pyr) in the J_{pdh} flux directly rather than through the cytosolic glucose concentration. We note that the simplification presented here is similar in spirit to that given in Bertram et al. (13).

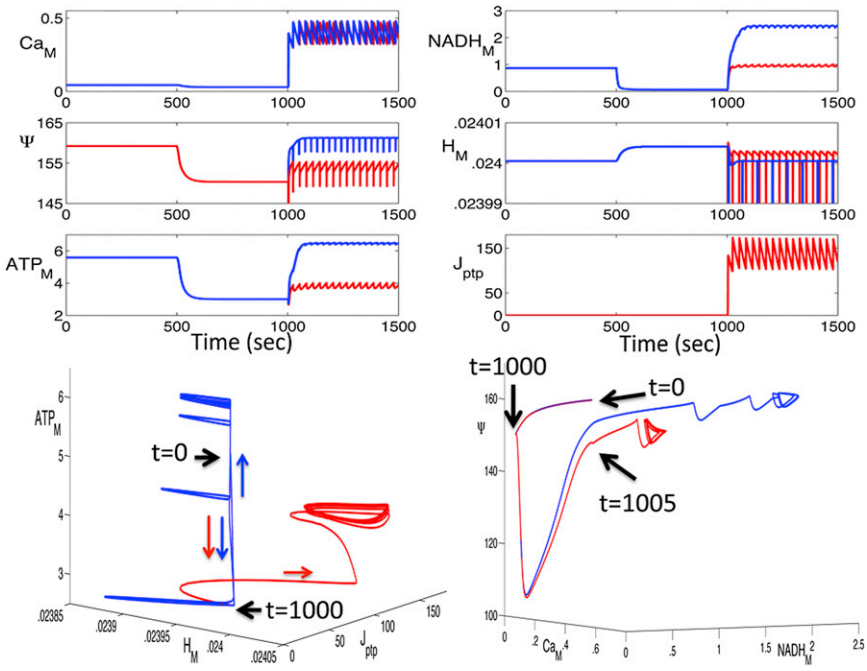

FIGURE 8 (*Top*) Time courses of the dependent variables and the PTP flux when the PTP is (*red*, $\phi_H = 5000$) and is not (*blue*, $\phi_H = 0$) present. Addition of the PTP leads to lower values of $\Delta\Psi$, $[ATP]_m$, and $[NADH]_m$ and higher values of $[H]_m$ during the recovery phase. (*Bottom*) Projections of the solutions shown on top onto two separate phase spaces. Very shortly after 2MeSADP is applied at $t = 1000$ s, there is a sharp drop followed by a fast recovery of $[H]_m$ and Ψ. Opening of the PTP, however, prevents Ψ from fully recovering, leading to lower values of mitochondrial ATP.

Analysis

We used mathematical analysis to derive precise conditions on model parameters for when either a decrease in pyruvate or external oxygen levels leads to a decrease in mitochondrial ATP production, and when this decrease in ATP production can be reversed by $P2Y_1R$ stimulation. To simplify the analysis, we do not include the K_{ATP} channel or the permeability transition pore. We also treat both pore-space cytosolic Ca^{2+} and mitochondrial oxygen levels as constant. We will determine how ATP production depends on changes in these constants. Here we are assuming that the role of $P2Y_1R$ stimulation is to increase the parameter corresponding to $[Ca]_{ps}$.

To simplify the notation, we write N, C, Ψ, and A instead of $[NADH]_m$, $[Ca]_m$, $\Delta\Psi$, and $[ADP]_m$, respectively. We use dot notation for time derivatives, and prime notation for differentiation with respect to a parameter. The reduced Magnus-Keizer model for the mitochondrial variables can then be written as

$$\begin{aligned} \dot{N} &= F_N(N,C,\Psi)/K_N, \\ \dot{C} &= F_C(C,\Psi)/K_C, \\ \dot{\Psi} &= F_\Psi(N,C,\Psi,A)/K_\Psi, \\ \dot{A} &= F_A(\Psi,A)/K_A, \end{aligned} \tag{22}$$

where K_N, K_C, K_Ψ, and K_A are constants and

$$\begin{aligned} F_N &= J_{pdh} - J_o, \\ F_C &= J_{uni} - J_{nc}, \\ F_\Psi &= J_{hres} - J_{hf1} - J_{ant} - J_{hl} - 2J_{uni} + J_{nc}, \\ F_A &= J_{ant} - J_{ptca} - J_{pf1}. \end{aligned} \tag{23}$$

Suppose that μ is some model parameter, such as Pyr, $[Ca]_{ps}$, or external oxygen level, for example. Moreover, when $\mu = \mu_0$, there is a fixed point

$$(N(\mu_0), C(\mu_0), \Psi(\mu_0), A(\mu_0))$$

of Eq. 22 that changes in a smooth way as we change the parameter μ. That is, there is a smooth curve ($N(\mu)$, $C(\mu)$, $\Psi(\mu)$, and $A(\mu)$) of fixed points that passes through the fixed point when $\mu = \mu_0$. We wish to determine whether ADP_m levels go up or down as we change μ; that is, we wish to compute the derivative $A'(\mu_0)$.

Note that at a fixed point, the right-hand sides of the four expressions in Eq. 22 are all zero. Setting these equal to zero, differentiating the equations with respect to μ, and then setting $\mu = \mu_0$ gives a system of linear equations of the form

$$\begin{bmatrix} a_1 & a_2 & a_3 & 0 \\ 0 & b_2 & b_3 & 0 \\ c_1 & c_2 & c_3 & c_4 \\ 0 & 0 & d_3 & d_4 \end{bmatrix} \begin{bmatrix} N'(\mu_0) \\ C'(\mu_0) \\ \Psi'(\mu_0) \\ A'(\mu_0) \end{bmatrix} = - \begin{bmatrix} \partial F_N/\partial\mu \\ \partial F_C/\partial\mu \\ \partial F_\Psi/\partial\mu \\ \partial F_A/\partial\mu \end{bmatrix}. \tag{24}$$

The entries in the 4×4 matrix correspond to the partial derivatives of the nonlinear functions in Eq. 22. In particular, $\alpha_i = \partial F_X/\partial Y$ where $X = N$, C, Ψ, or A if $\alpha = a$, b, c, or d, respectively, and $Y = N$, C, Ψ, or A if $i = 1$, 2, 3, or 4, respectively. Fig. 9 depicts the relationships among the variables and input parameters in the SMK model diagrammatically.

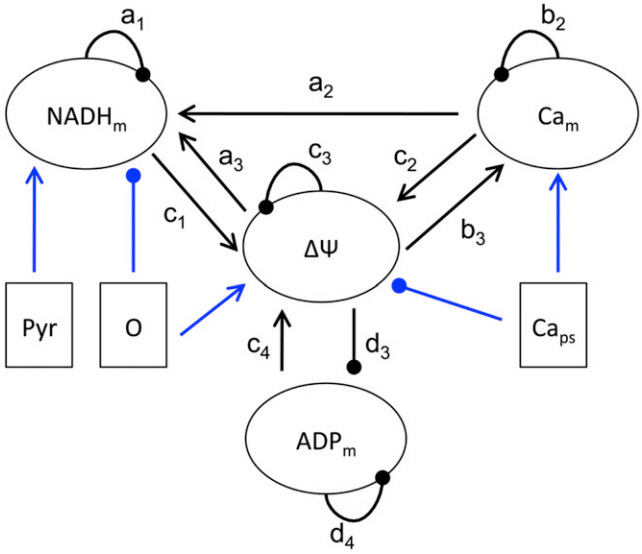

FIGURE 9 Schematic of the simplified Magnus-Keizer model. The connections represent relationships between the state variables and input parameters. (*Arrowheads* and *solid circles*) Positive and negative coupling, respectively.

Note that F_A does not depend on any of the input parameters. Hence, $\partial F_A/\partial\mu = 0$ and

$$A'(\mu_0) = -\left(\frac{d_3}{d_4}\right)\Psi'(\mu_0). \tag{25}$$

For the reduced model, d_3 and d_4 are both negative. It follows that $A'(\mu_0)$ and $\Psi'(\mu_0)$ have opposite signs. Because $ADP_m + ATP_m$ is constant, this implies that $ATP'_m(\mu_0)$ and $\Psi'(\mu_0)$ have the same sign. In what follows, we will determine $\Psi'(\mu_0)$. This then determines whether mitochondrial ATP levels increase or decrease with respect to a given parameter.

Dependence of ΔΨ on pyruvate

Let $\mu = \text{Pyr}$. The only flux that depends on Pyr is J_{pdh}; hence,

$$\frac{\partial F_C}{\partial\mu} = \frac{\partial F_A}{\partial\mu} = \frac{\partial F_\Psi}{\partial\mu} = 0.$$

Solving Eq. 24 for $\Psi'(\mu_0)$, we find that

$$\Psi'(\mu_0) = \frac{b_2c_1}{D}\frac{\partial F_N}{\partial\mu} = \frac{b_2c_1}{D}\frac{\partial J_{pdh}}{\partial Pyr}, \tag{26}$$

where

$$D = a_1\left(b_2c_3 - b_3c_2 - \frac{b_2c_4d_3}{d_4}\right) + c_1(a_2b_3 - a_3b_2). \tag{27}$$

It is not hard to show that $b_2 < 0$, $c_1 > 0$, and $\partial J_{pdh}/\partial Pyr > 0$. We assume that

$$D<0. \tag{28}$$

We have verified numerically that this is indeed the case, as shown in Fig. S4. It then follows that $\Psi'(\mu_0)$ is always positive; that is, mitochondrial ATP production always increases with pyruvate input.

Dependence of ΔΨ on Ca_{ps}

We next assume that $\mu = Ca_{ps}$, the pore-space Ca^{2+} level. The only flux that depends on Ca_{ps} is J_{uni}. It follows that $\partial F_C/\partial\mu = \partial F_A/\partial\mu = 0$ and $\partial F_\Psi/\partial\mu = -2\,\partial F_C/\partial\mu$. Solving Eq. 24 for $\Psi'(\mu_0)$, we find that

$$\Psi'(\mu_0) = \frac{\partial F_C}{\partial\mu}\left(\frac{a_1(c_2 + 2b_2 - \gamma)}{D}\right), \tag{29}$$

where

$$\gamma = \frac{a_2c_1}{a_1} \tag{30}$$

and D was defined in Eq. 27. We continue to assume that $D < 0$. It is not hard to show that $a_1 < 0$ and

$$\frac{\partial F_C}{\partial\mu} = \frac{\partial J_{uni}}{\partial Ca_{ps}} > 0. \tag{31}$$

Moreover,

$$\begin{aligned} c_2 + 2b_2 &= -2\frac{\partial J_{uni}}{\partial C} + \frac{\partial J_{nc}}{\partial C} + 2\left(\frac{\partial J_{uni}}{\partial C} - \frac{\partial J_{nc}}{\partial C}\right) \\ &= -\frac{\partial J_{nc}}{\partial C}. \end{aligned} \tag{32}$$

It then follows from Eq. 29 that

$$\Psi'(\mu_0) > 0 \text{ if and only if } \gamma < -\frac{\partial J_{nc}}{\partial C}. \tag{33}$$

We note that entry of Ca^{2+} into the mitochondria has two opposing effects on the potential: one is that the flux of positive ions depolarizes the membrane; the second is that increased mitochondrial Ca^{2+} increases $NADH_m$ leading to hyperpolarization. Because ρ_{nc} is closely related to the first effect, whereas γ is closely related to the second, we interpret Eq. 33 as giving a precise statement for when the hyperpolarizing effect of increased $NADH_m$ dominates the depolarizing effect of positive ions entering the mitochondrion.

In Fig. 10, *A* and *B*, we show bifurcation diagrams for $\Delta\Psi(Ca_{ps})$ and $ADP_m(Ca_{ps})$, respectively. Note that $\Delta\Psi(Ca_{ps})$ increases for small values of Ca_{ps} until $Ca_{ps} \approx 0.5$ and then decreases, whereas ADP_m first decreases and then increases. For the reduced model,

$$\frac{\partial J_{nc}}{\partial C} = \rho_{nc} = 3.$$

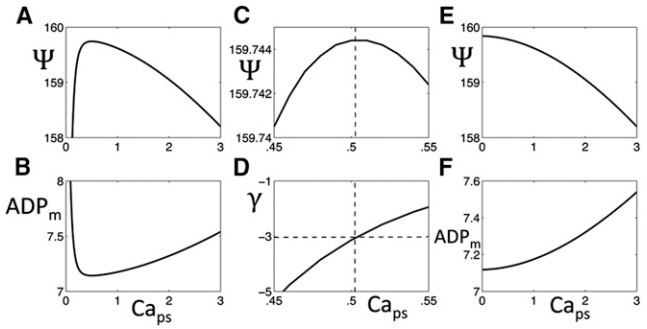

FIGURE 10 Bifurcation diagrams of the fixed points of Eq. 22 with bifurcation parameter Ca_{ps}. (*A*) The dependence of $\Delta\Psi$ on Ca_{ps}. (*B*) The dependence of $[ADP]_m$ on Ca_{ps}. (*C*) Detail near the maximum in panel *A*. (*D*) The function γ defined in the text. Note that $\gamma = -3$ at the value of Ca_{ps} where $\Delta\Psi$ reaches its maximum. (*E* and *F*) Here, the parameter $k_2 = 0$ and both $\Delta\Psi(Ca_C)$ and $ADP_m(Ca_{ps})$ are monotonic.

Hence, according to Eq. 33, $\Psi(Ca_{ps})$ should increase if $\gamma < -3$ and decrease if $\gamma > -3$. In Fig. 10, *C* and *D*, we plot $\Delta\Psi(Ca_{ps})$ for $0.45 < Ca_{ps} < 0.55$ as well as $\gamma(Ca_{ps})$ over this range. Note that $\Delta\Psi$ does indeed increase whenever $\gamma < -3$ and decreases for $\gamma > -3$.

Note that if $a_2 = \partial F_N/\partial C = 0$, then $\gamma = 0$. This corresponds to when the stimulatory effect of Ca_{ps} on PDH activity is saturated. In this case, Ψ (and, therefore, ATP_m) must be a decreasing function of Ca_{ps}. In Fig. 10, *E* and *F*, $k_2 = 0$, in which case F_N does not depend on Ca_m and $a_2 = 0$. The figures are consistent with the analysis, which predicts that $\Delta\Psi$ should always decrease, whereas ADP_m should increase.

Dependence of $\Delta\Psi$ on oxygen

Now assume that $\mu = O$, the mitochondrial oxygen level, which we assume to be constant. The two fluxes that depend on O are J_o and J_{hres}. Hence, $\partial F_C/\partial\mu = \partial F_A/\partial\mu = 0$. Let

$$\alpha = \frac{\partial F_N}{\partial O} \quad \text{and} \quad \beta = \frac{\partial F_\Psi}{\partial O}. \tag{34}$$

Solving Eq. 24 for $\Psi'(\mu_0)$, we find that

$$\Psi'(\mu_0) = \frac{b_2(\alpha c_1 - \beta a_1)}{D}, \tag{35}$$

where D is as before. It is not hard to show that $b_2 < 0$. We assume, as before, that $D < 0$. Then,

$$\Psi'(\mu_0) > 0 \text{ if and only if } \alpha c_1 - \beta a_1 > 0. \tag{36}$$

Now,

$$\alpha = -\frac{\partial J_o}{\partial O} = -\frac{k_3 k_o}{(k_o+O)^2}\left(\frac{N}{N+k_4N_{tot}}\right)\left(\frac{1}{1+k_{13}e^{0.191(\Psi-\Psi_3)}}\right),$$

$$\beta = \frac{\partial J_{hres}}{\partial O} = \frac{k_9 k_o}{(k_o+O)^2}\left(\frac{N}{N+k_{10}N_{tot}}\right)\left(\frac{1}{1+k_{11}e^{0.191(\Psi-\Psi_2)}}\right),$$

$$a_1 = \frac{\partial\left(J_{pdh}-J_o\right)}{\partial N}$$

$$= -\frac{k_3k_4N_{tot}}{(N+k_4N_{tot})^2}\left(\frac{O}{k_o+O}\right)\left(\frac{1}{1+k_{13}e^{0.191(\Psi-\Psi_3)}}\right)+\frac{\partial J_{pdh}}{\partial N},$$

$$c_1 = \frac{\partial J_{hres}}{\partial N} = \frac{k_9k_{10}N_{tot}}{(N+k_{10}N_{tot})^2}\left(\frac{O}{k_o+O}\right)\left(\frac{1}{1+k_{11}e^{0.191(\Psi-\Psi_2)}}\right). \tag{37}$$

In the reduced model, $k_{11} = k_{13}$ and $\Psi_2 = \Psi_3$. It follows that $\Psi'(\mu_0) > 0$ if and only if

$$1 < \frac{k_4}{k_{10}}\left(\frac{N+k_{10}N_{tot}}{N+k_4N_{tot}}\right) - \frac{k_9}{k_3}\left(\frac{N+k_4N_{tot}}{N+k_{10}N_{tot}}\right)\Omega, \tag{38}$$

where

$$\Omega = \frac{\partial J_{pdh}}{\partial N}\Big/\frac{\partial J_{hres}}{\partial N} < 0.$$

In particular,

$$\Psi'(\mu_0) > 0 \text{ if } 1 < \frac{k_4}{k_{10}}\left(\frac{N+k_{10}N_{tot}}{N+k_4N_{tot}}\right) \text{ or } k_{10} < k_4. \tag{39}$$

Note that in the modified Magnus-Keizer model, the two fluxes that depend on oxygen are the oxygen consumption, J_O, and respiration, J_{hres}. An increase in the oxygen consumption tends to depolarize the membrane, whereas an increase in respiration tends to hyperpolarize the membrane. The constants k_4 and k_{10} are closely related to how fast these fluxes change with respect to $NADH_m$. The analysis demonstrates that whether Ψ (and, therefore, ATP_m) is an increasing or decreasing function of oxygen input depends on the relative sizes of these two parameters.

Fig. 11, *A* and *B*, shows bifurcation diagrams for $\Delta\Psi$ and ADP_m, respectively; the bifurcation parameter is O. Note the $\Delta\Psi$ is monotone-increasing, whereas ADP_m is monotone-decreasing. Hence, ATP_m is monotone-increasing. This is consistent with the analysis because $k_{10} = 0.43 < 0.74 = k_4$.

If $k_{10} > k_4$, then Ψ and ATP_m may be either increasing or decreasing functions of O, depending on the other parameters. Fig. 11 *C* shows an example with ADP_m first decreasing and then increasing as O increases. If we let Γ denote the right-hand side of Eq. 38, then the minimum value of ADP_m should be when $\Gamma = 1$. In Fig. 11 *D*, we show that this is indeed the case.

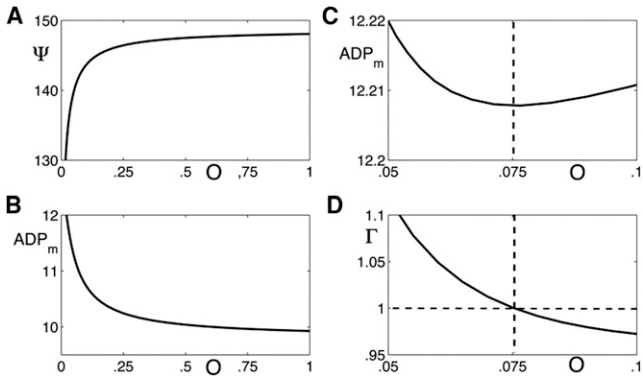

FIGURE 11 Bifurcation diagrams of the fixed points of Eq. 22 with bifurcation parameter O. (*A*) The dependence of $\Delta\Psi$ on O. (*B*) The dependence of ADP_m on O. (*C*) Here, $k_{10} = 1$ and $k_4 = 0.33$. The dependence of ADP_m on O is no longer monotonic. (*D*) The function Γ defined in the text. Note that $\Gamma = 1$ at the value of O where ADP_m has its minimum value.

DISCUSSION

One of the primary goals of this article was to develop a mathematical model that supports recent experimental results showing that, in mouse cortical astrocytes, the magnitude of ischemic lesions and cytotoxic edema can be significantly reduced by stimulating $P2Y_1Rs$ (4,5). Consistent with experiments, the model demonstrates that the protective role of $P2Y_1R$ stimulation results from increased IP_3-mediated Ca^{2+} release, which, in turn, leads to increased mitochondrial ATP production.

The mathematical model modifies, extends, and integrates several earlier models for different aspects of the relevant cellular processes. Following Fall and Keizer (6), the model combines the Li-Rinzel model for ER Ca^{2+} handling with the Magnus-Keizer model for mitochondrial Ca^{2+} handling and ATP production. We then added equations for cell volume, membrane potential, and concentrations of ionic species. We modeled the dependence of IP_3 production on $P2Y_1R$ stimulation as in Di Garbo et al. (17) and modified the rate at which NADH is produced by the citric-acid cycle in the Magnus-Keizer model as in Bertram et al. (13). We then added differential equations for the mitochondrial oxygen level and pH, because these are assumed to be static in the Magnus-Keizer model. Finally, we added models for a mitochondrial K_{ATP} channel and the permeability transition pore to the Magnus-Keizer model to explore their possible roles in neuroprotection. These were modeled as in Bertram et al. (14), Magnus and Keizer (15), and Oster et al. (12), respectively.

A second primary goal was to analyze the model to gain insights into the underlying biological data. The analysis leads to precise conditions on model parameters for how variations in IP_3-mediated Ca^{2+} release, oxygen levels, and pyruvate affect mitochondrial ATP production. It is especially important to understand conditions for when increasing cytosolic Ca^{2+} levels lead to increased mitochondrial ATP production, because this forms the basis of the proposed mechanism underlying neuroprotection. We note that experiments involving other systems have demonstrated that this is not always the case; that is, higher cytosolic Ca^{2+} levels can, in fact, lead to a decrease in ATP production (see, for example, Eq. 13).

Simulations of the model, along with the analysis, lead to concrete predictions that one may be able to test experimentally. As Fig. 10 demonstrates, the dependence of $\Delta\Psi$ and ATP_m on Ca_{ps} is typically not monotonic; that is, ATP levels reach a maximum value at some moderate level of Ca_{ps}. It would be interesting to test experimentally whether there is indeed a nonmonotonic dependence of ATP production on Ca_{ps} and, if so, whether the maximum level of ATP production and the value of Ca_{ps} at which this occurs is similar to that predicted by the analysis. The analysis and simulations also demonstrate that $P2Y_1R$ stimulation may be accompanied with oscillations in ER and mitochondrial Ca^{2+}. There should also be oscillations in cytosolic Ca^{2+}; however, these may only be observed in the pore space between the ER and mitochondria. Finally, our results suggest that one reason why neurons are considerably more vulnerable to changes in ischemic conditions than astrocytes may be because of the PTP, which appears to play a more prominent role in neurons than in astrocytes.

Although the model is quite complicated, it should still be considered as minimal in the sense that it includes only those fluxes and cellular processes needed to reproduce and account for the experimental results. For example, the model includes just three plasma membrane ionic fluxes and one pump, although other ions such as glutamate, as well as other pumps and transporters, surely play a critical role in ischemia. We also approximate the concentration of external potassium ions as constant. To model spreading depression and excitability in a network of neurons and astrocytes accurately, incorporating the dynamics of $[K^+]_o$ would be critically important (27,28). Moreover, although the Magnus-Keizer model has proven very useful for understanding many aspects of mitochondrial Ca^{2+} handling and ATP production, it clearly does not (and cannot) take into account the myriad of complex processes involved in cellular respiration and energy production. For example, we do not consider glycolytic oscillations (14) or gluconeogenesis (29). Our hope is that the model and analysis presented here can serve as useful beginnings to which more detailed processes, such as the reaction-diffusion dynamics involved in stroke propagation, can be added. Such physiologically based computational tools have the potential to transform and help drive ischemia research.

SUPPORTING MATERIAL

Additional information and five figures are available at http://www.biophysj.org/biophysj/supplemental/S0006-3495(13)00242-7.

The authors thank the Mathematical Biosciences Institute at The Ohio State University and the National Science Foundation supported Computational Cell Biology course at Cold Spring Harbor Laboratory for facilitating our collaboration.

This research has been supported by the National Institutes of Health under National Institute for Aging grant No. AG29461 (to J.D.L.) and National Institute of Mental Health grant No. MH64611 (to C.P.F.), and by the National Science Foundation under Division of Mathematical Sciences grants No. 0718558 (to C.P.F.), No. 1022627 (to D.T.), and No. 0931642 (to the Mathematical Biosciences Institute).

REFERENCES

1. Kimelberg, H. K. 2005. Astrocytic swelling in cerebral ischemia as a possible cause of injury and target for therapy. *Glia.* 50:389–397.
2. Liang, D., S. Bhatta, …, J. M. Simard. 2007. Cytotoxic edema: mechanisms of pathological cell swelling. *Neurosurg. Focus.* 22:E2.
3. Rosenblum, W. I. 2007. Cytotoxic edema: monitoring its magnitude and contribution to brain swelling. *J. Neuropathol. Exp. Neurol.* 66: 771–778.
4. Zheng, W., L. T. Watts, …, J. D. Lechleiter. 2010. Purinergic receptor stimulation reduces cytotoxic edema and brain infarcts in mouse induced by photothrombosis by energizing glial mitochondria. *PLoS ONE.* 5:e14401.
5. Wu, J., J. D. Holstein, …, J. D. Lechleiter. 2007. Purinergic receptor-stimulated IP_3-mediated Ca^{2+} release enhances neuroprotection by increasing astrocyte mitochondrial metabolism during aging. *J. Neurosci.* 27:6510–6520.
6. Fall, C. P., and J. E. Keizer. 2001. Mitochondrial modulation of intracellular Ca^{2+} signaling. *J. Theor. Biol.* 210:151–165.
7. Magnus, G., and J. E. Keizer. 1997. Minimal model of β-cell mitochondrial Ca^{2+} handling. *Am. J. Physiol.* 273:C717–C733.
8. Li, Y. X., and J. Rinzel. 1994. Equations for $InsP_3$ receptor-mediated $Ca^{2+}{}_i$ oscillations derived from a detailed kinetic model: a Hodgkin-Huxley like formalism. *J. Theor. Biol.* 166:461–473.
9. O'Rourke, B. 2004. Evidence for mitochondrial K^+ channels and their role in cardioprotection. *Circ. Res.* 94:420–432.
10. Fryer, R. M., J. T. Eells, …, G. J. Gross. 2000. Ischemic preconditioning in rats: role of mitochondrial K_{ATP} channel in preservation of mitochondrial function. *Am. J. Physiol. Heart Circ. Physiol.* 278: H305–H312.
11. Goldberg, M. P., and D. W. Choi. 1993. Combined oxygen and glucose deprivation in cortical cell culture: calcium-dependent and calcium-independent mechanisms of neuronal injury. *J. Neurosci.* 13:3510–3524.
12. Oster, A. M., B. Thomas, …, C. P. Fall. 2011. The low conductance mitochondrial permeability transition pore confers excitability and CICR wave propagation in a computational model. *J. Theor. Biol.* 273:216–231.
13. Bertram, R., M. Gram Pedersen, …, A. Sherman. 2006. A simplified model for mitochondrial ATP production. *J. Theor. Biol.* 243:575–586.
14. Bertram, R., L. Satin, …, A. Sherman. 2004. Calcium and glycolysis mediate multiple bursting modes in pancreatic islets. *Biophys. J.* 87:3074–3087.
15. Magnus, G., and J. E. Keizer. 1998. Model of β-cell mitochondrial calcium handling and electrical activity. I. Cytoplasmic variables. *Am. J. Physiol.* 274:C1158–C1173.
16. Fall, C. P., J. M. Wagner, …, R. Nuccitelli. 2004. Cortically restricted production of IP_3 leads to propagation of the fertilization Ca^{2+} wave along the cell surface in a model of the *Xenopus* egg. *J. Theor. Biol.* 231:487–496.
17. Di Garbo, A., M. Barbi, …, M. Nobile. 2007. Calcium signaling in astrocytes and modulation of neural activity. *Biosystems.* 89:74–83.
18. Dronne, M. A., J. P. Boissel, and E. Grenier. 2006. A mathematical model of ion movements in grey matter during a stroke. *J. Theor. Biol.* 240:599–615.
19. Pokhilko, A. V., F. I. Ataullakhanov, and E. L. Holmuhamedov. 2006. Mathematical model of mitochondrial ionic homeostasis: three modes of Ca^{2+} transport. *J. Theor. Biol.* 243:152–169.
20. Jakobsson, E. 1980. Interactions of cell volume, membrane potential, and membrane transport parameters. *Am. J. Physiol.* 238:C196–C206.
21. Ermentrout, G. B., and D. H. Terman. 2010. Mathematical Foundations of Neuroscience. Springer, New York.
22. MATLAB. 2008. The MathWorks. Natick, MA.
23. Ermentrout, G. B. 2002. Simulating, Analyzing, and Animating Dynamical Systems: A Guide To XPPAUT for Researchers and Students. SIAM, Philadelphia, PA.
24. Lipton, P. 1999. Ischemic cell death in brain neurons. *Physiol. Rev.* 79:1431–1568.
25. Fall, C. P., and J. P. Bennett, Jr. 1999. Visualization of cyclosporin A and Ca^{2+}-sensitive cyclical mitochondrial depolarizations in cell culture. *Biochim. Biophys. Acta.* 1410:77–84.
26. Lin, D. T., J. Wu, …, J. D. Lechleiter. 2007. Ca^{2+} signaling, mitochondria and sensitivity to oxidative stress in aging astrocytes. *Neurobiol. Aging.* 28:99–111.
27. Tuckwell, H. C., and R. M. Miura. 1978. A mathematical model for spreading cortical depression. *Biophys. J.* 23:257–276.
28. Ullah, G., J. R. Cressman, Jr., …, S. J. Schiff. 2009. The influence of sodium and potassium dynamics on excitability, seizures, and the stability of persistent states. II. Network and glial dynamics. *J. Comput. Neurosci.* 26:171–183.
29. Ockner, R. 2004. Astrocyte metabolism and astrocyte-neuron interaction. *In* Integration of Metabolism, Energetics, and Signal Transduction Springer, New York.